Redox Biology 62 (2023) 102676

Contents lists available at ScienceDirect

Redox Biology

journal homepage: www.elsevier.com/locate/redox

Glutaredoxin 1 protects lens epithelial cells from epithelial-mesenchymal transition by preventing casein kinase 1α S-glutathionylation during posterior capsular opacification

Chenshuang Li [a,b], Xi Chen [b], Siqi Zhang [a,b], Chen Liang [a,b], Xiaopan Ma [c], Ruixue Zhang [c], Hong Yan [a,b,c,*]

[a] Department of Ophthalmology, The Second Affiliated Hospital of Xi'an Jiaotong University, Xi'an, 710004, Shaanxi Province, China
[b] Shaanxi Eye Hospital, Xi'an People's Hospital (Xi'an Fourth Hospital), Affiliated People's Hospital of Northwest University, Xi'an, 710004, Shaanxi Province, China
[c] Institute of Medical Research, Northwestern Polytechnical University, Xi'an, 710072, Shaanxi Province, China

ARTICLE INFO

Keywords:
Glutaredoxin 1
Epithelial-mesenchymal transition
Casein kinase 1α
S-glutathionylation
Posterior capsular opacification

ABSTRACT

Oxidative stress drives protein S-glutathionylation, which regulates the structure and function of target proteins and is implicated in the pathogenesis of many diseases. Glutaredoxin 1 (Grx1), a cytoplasmic deglutathionylating enzyme, maintains a reducing environment within the cell under various conditions by reversing S-glutathionylation. Grx1 performs a wide range of antioxidant activities in the lens and prevents protein-thiol mixed disulfide accumulation, reducing protein–protein aggregation, insolubilization, and apoptosis of lens epithelial cells. Oxidative stress is related to epithelial–mesenchymal transition (EMT) during posterior capsular opacification (PCO). However, whether Grx1-regulated protein S-glutathionylation plays an essential role in PCO remains unclear. In this study, we revealed that Grx1 expression was decreased in mice following cataract surgery. Furthermore, the absence of Grx1 elevated oxidative stress and protein S-glutathionylation and aggravated EMT in both *in vitro* and *in vivo* models. Concurrently, these results could be reversed by Grx1 overexpression. Notably, liquid chromatography–tandem mass spectrometry results showed that casein kinase 1α (CK1α) was susceptible to S-glutathionylation under oxidative stress, and CK1α S-glutathionylation (CK1α-SSG) was mediated at Cys249. The absence of Grx1 upregulated CK1α-SSG, subsequently decreasing the CK1α-induced phosphorylation of β-catenin at Ser45. The consequential downregulation of degradative β-catenin and upregulation of its nuclear translocation activated the Wnt/β-catenin signaling pathway and aggravated EMT. In conclusion, the downregulated expression of Grx1 in mice following cataract surgery aggravated EMT by upregulating the extent of CK1α-SSG. To the best of our knowledge, our study is the first to report how S-glutathionylation regulates CK1α activity under oxidative stress.

1. Introduction

Cataracts are the most common cause of blindness worldwide and have visually impaired approximately 95 million people. The only effective treatment for cataracts is surgery [1]; however, this is frequently complicated by long-term, postoperative, posterior capsular opacification (PCO) [2]. The incidence of PCO at one, three, and five years post-cataract surgery is 11.8%, 20.7%, and 28.4%, respectively [3]. The incidence of PCO is 20%–60% in adults [4] and can reach 95% or more in young people as the cells of adolescents and children have greater regenerative and proliferative capacities than the cells of adults [5]. PCO not only causes quantitative visual disturbances, but also reduces the quality of vision, leading to a reduction in contrast sensitivity, halo effect, and lack of binocular vision [6]. Although neodymium-doped yttrium aluminum garnet laser capsulotomy is used to treat postoperative PCO, it also has many risks, such as increased

Abbreviations: CK1α, casein kinase 1α; CK1α-SSG, casein kinase 1α S-glutathionylation; EMT, epithelial-mesenchymal transition; Grx, glutaredoxin; LECs, lens epithelial cells; PCO, posterior capsular opacification; Pro-SSG, protein-glutathione mixed disulfide adducts; TGF-β, transforming growth factor-β; α-SMA, α-smooth muscle actin; LC-MS/MS, liquid chromatography–tandem mass spectrometry.

* Corresponding author. Department of Ophthalmology, The Second Affiliated Hospital of Xi'an Jiaotong University, NO.157 Xiwu Rd, Xi'an, 710004, Shaanxi Province, China.
E-mail address: yan2128ts@med.nwu.edu.cn (H. Yan).

https://doi.org/10.1016/j.redox.2023.102676
Received 20 February 2023; Received in revised form 6 March 2023; Accepted 14 March 2023
Available online 24 March 2023

intraocular pressure, lens movement, lens pitting, and transient iritis or uveitis, cystoid macular edema, and retinal tear or detachment [7]. Therefore, it is vital to elucidate the mechanisms of PCO formation and development and to explore preventive strategies.

PCO is attributed to residual lens epithelial cells (LECs) migration, proliferation across the posterior capsule, and eventual differentiation into fibroblastic and lens fiber–like cells after cataract surgery [8]. This epithelial–mesenchymal transition (EMT) of LECs plays a critical pathogenic role in PCO [9]. It is generally accepted that transforming growth factor-β (TGF-β) is the upstream regulator of EMT [10,11] via Smad-dependent and Smad-independent signaling pathways [9,12]. However, growth factors and inflammatory cytokines accumulate in aqueous humor only for a short period, whereafter PCO continues to develop [13–15]. This suggests the involvement of complex pathways during PCO formation, particularly during its chronic phases. Furthermore, in the normal physiological state, the lens contains significantly higher levels of various antioxidant substances than the aqueous humor. However, cataract surgery exposes LECs to the aqueous humor, thereby reducing their antioxidant capacity [16] and exacerbating oxidative stress. Our previous *in vitro* and *in vivo* models have suggested that this imbalance activates Wnt/β-catenin signaling, resulting in EMT in LECs and the development of PCO [17,18].

Oxidative stress drives S-glutathionylation of free thiol groups (-SH) on the cysteine residues of proteins to form protein-glutathione mixed disulfide adducts (Pro-SSG) [19]. Protein S-glutathionylation is a reversible process that regulates the structure and function of target proteins including AKT [20], sirtuin-1 [21], mitofusin [22], GAPDH [23] and FABP5 [24]. Deglutathionylation is primarily catalyzed by glutaredoxin (Grx), a thiol-disulfide oxidoreductase. Mammalian cells encode two principal dithiol Grx isoforms: cytoplasmic Grx1 and mitochondrial or nuclear Grx2 [19]. Grx1 facilitates the regulation of various cellular functions and maintains the cellular redox state under various environmental conditions. Grx1-regulated protein S-glutathionylation has been implicated in the pathogenesis of cardiovascular diseases [25], neurodegenerative disorders [26], acute lung injury [24], and cancer [27,28]. Additionally, Grx1 mediates numerous antioxidant functions in the lens. Grx1 prevents protein-thiol mixed disulfide accumulation reducing protein–protein aggregation, insolubilization, and apoptosis of LECs [29]. As mentioned above, cataract surgery exposes LECs to aqueous humor, thereby significantly reducing LEC antioxidant capabilities. However, the involvement and the exact mechanism of Grx1-regulated protein S-glutathionylation in PCO remains unclear.

We found that Grx1 knockout (KO) mice developed more severe PCO after cataract surgery than control mice in preliminary experiment, suggesting the involvement of Grx1 and S-glutathionylation in PCO development. Furthermore, casein kinase 1α (CK1α) was among the top S-glutathionylation candidates identified by liquid chromatography–tandem mass spectrometry (LC-MS/MS) and validated using co-immunoprecipitation (Co-IP). CK1α has broad serine/threonine protein kinase activity and is one of the main components of the Wnt/β-catenin signaling pathway [30]. In addition, CK1α phosphorylates β-catenin at Ser45 as part of the β-catenin destruction complex, leading to its subsequent degradation [31]. Thus, CK1α acts as an essential negative regulator of Wnt/β-catenin signaling.

Here, we aimed to evaluate the involvement of Grx1-regulated CK1α S-glutathionylation (CK1α-SSG) in EMT of LECs and subsequent PCO development; and the mechanism by which S-glutathionylation regulates CK1α activity under oxidative stress. Our results will help in understanding the mechanism underlying the S-glutathionylation regulation of CK1α activity under oxidative stress.

2. Materials and methods

2.1. Mice

Grx1 KO mice (C57BL/6 N) were generated using CRISPR/Cas-mediated genome engineering by Cyagen Biosciences and were bred in an animal facility at Northwestern Polytechnical University. Control (C57BL/6 N) mice were purchased from the Laboratory Animal Center of Xi'an Jiaotong University. All animal experiments were performed according to protocols approved by the Institutional Animal Care and Use Committee of Northwestern Polytechnical University (Ethics code: 202001010). An equal number of male and female mice were randomly divided into different groups. All experiments involving the control and Grx1 KO mice were conducted by the same analyst, who was blinded to the conditions.

2.2. Mouse cataract surgery

The mice were subjected to cataract surgery as described by Lois et al. [32] and Wei et al. [17]. Both control and Grx1 KO mice (8 weeks old) were anesthetized by intraperitoneal injection of pentobarbital (40 mg/kg). After treatment with tropicamide eye drops, a 2 mm limbal incision was made. The fiber mass was gently removed by hydro-dissection using a 1 mL syringe fitted with a 32-gauge flat-tipped cannula. The remaining lens capsule was carefully washed and filled with phosphate-buffered saline (PBS) to remove any lens fiber debris and restore the ocular chamber morphology. Finally, the anterior chamber was filled with PBS. Unilateral surgical procedures were performed for all mice. Ofloxacin antibiotic eye drops were administered immediately after surgery and thrice daily. Mice were euthanized at specific times after surgery, whereafter the posterior lens capsules were isolated.

2.3. Cell culture and treatment

Human lens epithelial B3 (HLE-B3) cells were purchased from the American Tissue Culture Collection. The cells were grown in a minimum essential medium (Gibco, C11095500BT) containing 10% fetal bovine serum (FBS) (Lonsera, S711–001S). Cell cultures were maintained at 37 °C in a humidified 5% CO_2 incubator. Lentivirus-mediated Grx1 knockdown and overexpression vectors were purchased from GeneChem. Lentivirus-mediated constructs of the wild-type (WT) and cysteine mutant CK1α were purchased from GeneChem (C104S, C150S, C249S, C263S, TGT→TCT). The CK1α quadruple mutant (C104S, C150S, C249S, C263S) was as 4MUT.

Before transfection, HLE-B3 cells were inoculated in 6-well plates. The cells were infected with lentivirus at 50–60% confluence. After 8 h, the infected cells were supplemented with 10% FBS until they reached 100% confluency. Cells stably expressing the target genes were obtained by puromycin selection.

The cells were seeded 48 h before treatment to ensure proper cell adherence and stability. When the cells reached 70% confluency, they were starved for 12 h in a serum-free medium. After that, 20 μM hydrogen peroxide (H_2O_2) (Sigma, 323381) was added and cells were incubated at appropriate intervals.

2.4. Hematoxylin-eosin (HE) and immunofluorescence staining

Mouse eyeballs were fixed in 4% paraformaldehyde (PFA) for >24 h and then embedded in paraffin for HE staining according to standard protocols.

For immunofluorescence staining, cells grown on coverslips and posterior capsules isolated from the eyes were washed with PBS, fixed with 4% PFA, and permeabilized using 0.3% Triton-X100 (Beyotime, ST795) at room temperature. Next, cells and capsules were blocked for 1 h at room temperature with a blocking buffer prepared in PBS with 5% normal donkey serum (Solarbio, SL050). The primary antibodies (Abcam), namely α-smooth muscle actin (α-SMA; ab5694, 1:400), vimentin (ab20346, 1:1000), β-catenin (ab16051, 1:500), GSH (ab19534, 1:50), and Grx1 (ab45953, 1:50), were applied in PBS and incubated at 4 °C overnight in a humid chamber. The secondary

antibodies (Abbkine, 1:200), namely green donkey anti-rabbit IgG (A24221), green donkey anti-mouse IgG (A24211), red donkey anti-rabbit IgG (A24421), and red donkey anti-mouse IgG (A24411) were applied and incubated at room temperature for 2 h in a humid chamber. The nuclei were stained with DAPI (Yeasen, 40728ES03, 5 μg/mL). Finally, the coverslips were mounted with an anti-fluorescence quenching solvent (Beyotime, P0126) and observed using a confocal laser scanning microscope (Olympus).

2.5. Western blotting

After washing the cells with ice-cold PBS, lysis buffer (Beyotime, P0013B) containing 1% phenylmethylsulfonyl fluoride (Beyotime, ST506) was added. Protein concentrations were assessed using a bicinchoninic acid protein assay kit (Beyotime, P0010). Equal amounts of protein were separated by 8–12% sodium dodecyl sulfate-polyacrylamide gel electrophoresis, transferred to polyvinylidene fluoride membranes (PVDF; Millipore, ISEQ00010/IPVH00010), and blocked in Tris-buffered saline with 0.1% Tween-20 (TBST) containing 5% nonfat powdered milk (Beyotime, P0216). The PVDF membranes were incubated overnight at 4 °C with the following primary antibodies: α-SMA (Abcam, ab5694, 1:1000), vimentin (Abcam, ab20346, 1:1000), E-cadherin (Proteintech, 60335-1, 1:5000), N-cadherin (Proteintech, 66219-1, 1:5000), Grx1 (Abcam, ab45953, 1:1000), GSK-3β (CST, 12456, 1:1000), Axin1 (ABclonal, A16019, 1:1000), CK1α (ABclonal, A16225, 1:1000), DSTN (Abcam, ab186754, 1:1000), GSH (Abcam, ab19534, 1:1000), β-catenin (Abcam, ab16051, 1:4000), phospho-β-catenin (Ser45) (ABclonal, AP0580, 1:1000), β-actin (Proteintech, 66009, 1:5000), and LaminB (ABclonal, A16909, 1:1000). The membranes were incubated for 1.5 h at room temperature with either horseradish peroxidase (HRP)-conjugated Affinipure goat anti-mouse IgG (H + L) (Proteintech, SA00001-1, 1:5000) or HRP-conjugated Affinipure goat anti-rabbit IgG (H + L) (Proteintech, SA00001-2, 1:5000) secondary antibodies. Immunoreactive bands were developed using ECL chemiluminescence (Beijing 4A Biotech, 4AW011-100) and visualized with a ChemiDoc XRS System (Bio-Rad). The resulting protein bands were analyzed using ImageJ software. LaminB and β-actin were used as internal controls. Nuclear and cytoplasmic fractions were separated using a nuclear and cytoplasmic extraction kit (Beyotime, P0028).

2.6. GSH and GSSG concentration determination

A GSH and GSSG assay kit (Beyotime, S0053) was used for quantification according to the manufacturer's protocol (Beyotime, P0012). The GSH to GSSG ratio (GSH/GSSG) was subsequently calculated.

2.7. Real-time polymerase chain reaction (qPCR)

Total RNA was extracted using TRIzol reagent (TaKaRa, 9108), and quantified using an ultramicro-spectrophotometer (Denovix). Total RNA (500 ng) served as a template to synthesize cDNA using the PrimeScript RT Reagent Kit (Takara, RR820A). For real-time PCR (RT-PCR), TB Green Premix Ex Taq II (TaKaRa, RR036A) was used for target gene amplification and the CFX96 Touch RT-PCR Detection System (Bio-Rad) was used for data collection. β-actin served as an internal control. All primers were synthesized by Tsingke and their sequences are listed in the Supplementary Table 1.

2.8. Wound healing assay

Cells were seeded into 6-well plates and cultured to 80–90% confluency. Cells were scratched using a sterile plastic pipette tip (200 μL) and washed with PBS to remove debris. After that, 1% FBS medium was added to each well with or without H_2O_2 (20 μM). Wounded areas were imaged after 0 h, 24 h, and 48 h of incubation and measured using ImageJ software. The data were quantified as follows: cell migration percentage = (original scratch area – new scratch area)/original scratch area.

2.9. Transwell migration assay

Cells (3×10^4) were seeded into the upper compartment of an 8 μm pore size 24-well transwell chamber (Falcon, 353097) with 200 μL serum-free medium. The lower chamber contained 600 μL medium supplemented with 15% FBS. After 48 h of incubation, cells in the upper chamber were mechanically removed. The migrated cells were fixed with 4% PFA for 30 min and subsequently stained with 1% crystal violet (Beyotime, C0121) for 15 min at room temperature. The number of migrated cells was measured by counting five fields of vision.

2.10. EdU staining assay

A BeyoClick EdU Cell Proliferation Kit with Alexa Fluor 488 and 594 (Beyotime, C0071S and C0078S) was used according to the manufacturer's protocol. Cells were seeded onto coverslips inserted in 24-well plates. At 50% confluency, H_2O_2 (20 μM) was added and cells were starved overnight in serum-free medium before being incubated for 24 h. After that, 10 μM EdU was added, and cells were incubated for 8 h before harvesting. Slides were observed using fluorescence microscopy.

2.11. LC-MS/MS

Six dishes of cells were seeded in advance in each well. H_2O_2 (20 μM) was randomly added to three dishes, and serum-free medium was added to the remainder, whereafter, all dishes were incubated for 24 h. The cells were harvested, and lysis buffer (Beyotime, P0013B) containing 1% phenylmethylsulfonyl fluoride (Beyotime, ST506) was added (30 min on ice). The lysates were centrifuged (13,000×*g*, 10 min, 4 °C), and the soluble protein fraction was retained. The protein concentration was determined using the BCA method. In total, 50 μg sample was transferred to a new EP tube and adjusted to a final volume of 100 μL with 50 mM NH_4HCO_3 (Sigma–Aldrich). Iodoacetamide (IAA, Sigma–Aldrich) solution was added to a final concentration of 50 mmol/L and protected from light for 40 min. Six volumes (approximately 600 μL) of pre-cooled (−20 °C) acetone (Sigma–Aldrich), frozen at −20 °C was added to the solution, and the sediment was allowed to freeze overnight. The sample was centrifuged at 8000×*g*, 4 °C for 10 min, the EP pipe was carefully invert, and the acetone was poured out; the white sediment was retained, and the sediment was allowed to dry for 2–3 min. Solubilized protein was precipitated with 100 μL NH_4HCO_3 (50 mM). In total, 1 μg trypsin (Promega) was added, and the sample was digested overnight at 37 °C. After digestion, the peptide was desalted using a self-priming desalting column, and the solvent was evaporated in a vacuum centrifuge at 45 °C. The peptide was dissolved in the sample solution (0.1% formic acid (FA, Sigma–Aldrich) containing 2% acetonitrile (ACN, Fisher Chemical)), vortexed thoroughly, and centrifuged at 13200 rpm for 10 min at 4 °C; the supernatant was transferred to the sample tube for mass spectrometry analysis. The Easy-nLC 1200 system (Thermo Fisher Scientific, USA) was used, and the nanocolumn, 150 μm × 15 cm in size, was constructed in-house and packed with Acclaim PepMap RPLC C18 (1.9 μm, 100 Å, Dr. Maisch GmbH, Germany). The loaded sample volume was 5 μL, mobile phase A was 0.1% FA in water, mobile phase B was 0.1% FA in water (20%) and ACN (80%), and the total flow rate was 600 nL/min. LC linear gradient was from 4% to 10% B for 5 min, from 10% to 22% B for 80 min, from 22% to 40% B for 25 min, from 40% to 95% B for 5 min, and from 95% to 95% B for 5 min. OrbitrapEclipse Mass Spectrometer (Thermo Fisher Scientific, USA) was used [spray voltage: 2.2 kV, capillary temperature: 270 °C]. MS parameters was resolution: 70000 at 400 *m/z*, precursor *m/z* range: 300.0–1400.0. MS/MS parameters were product ion scan range starting from *m/z* 50, activation type: HCD, normalized coll. energy: 30.0, and activation time: 120.000. Data-dependent MS/MS was up to the top 20 most intense peptide ions

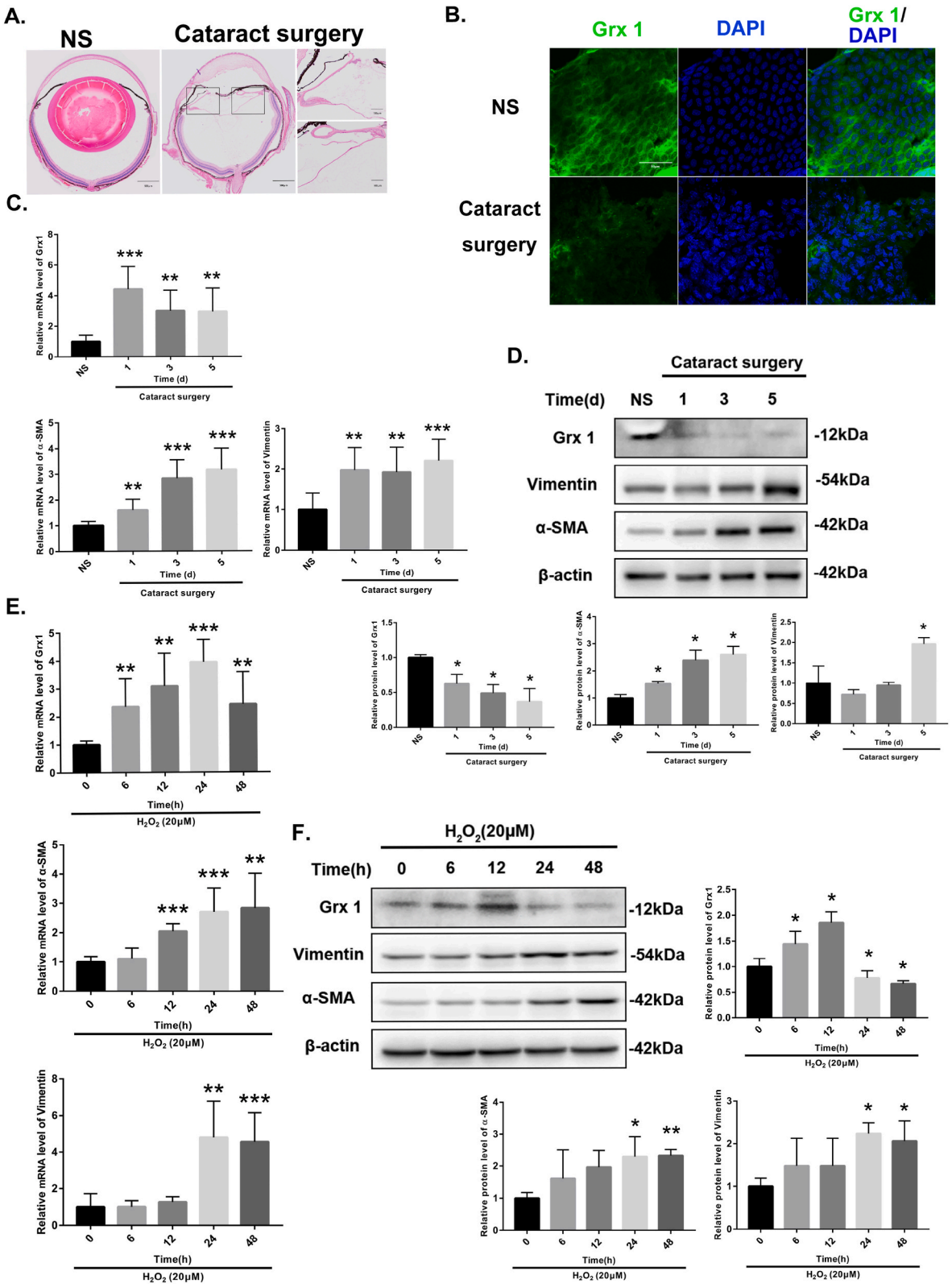

Fig. 1. Grx1 was downregulation both *in vivo* and *in vitro experiments*.
(A) HE staining of bulbus oculi showed capsular manifestations 1 day after surgery and NS group. (B) Immunofluorescence staining of lens capsules of the NS group and 5 days after surgery. Nuclei were counterstained with DAPI (blue). Grx1 presented as green, fluorescent light. (C) The Grx1, α-SMA and vimentin mRNA level of NS group and 1, 3 and 5 days after surgery by qPCR. (D) Western blotting indicating Grx1, α-SMA and vimentin protein levels for the NS group and 1, 3 and 5 days after surgery. (E) The Grx1, α-SMA and vimentin mRNA expression level after H_2O_2 (20 μM)-treated LECs 0 h, 6 h, 12 h, 24 h, and 48 h by qPCR. (F) Western blotting indicating Grx1, α-SMA and vimentin protein levels after H_2O_2 (20 μM)-treated LECs 0 h, 6 h, 12 h, 24 h, and 48 h. Columns represent the mean ± SEM, n = 3, *P < 0.05, **P < 0.01, ***P < 0.001.

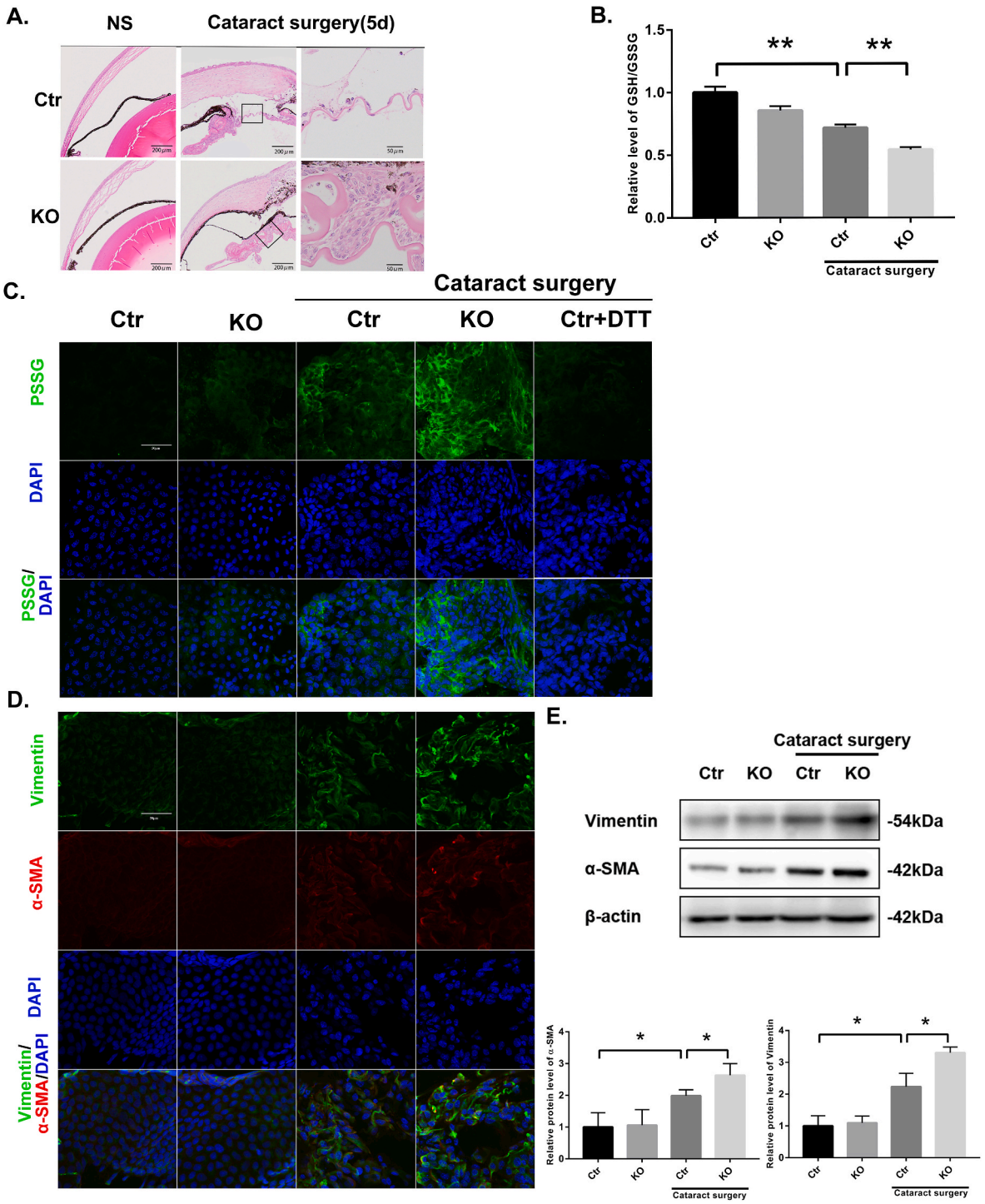

Fig. 2. Grx1 KO mice was more susceptible to PCO.
(A) HE staining of bulbus oculi showed different anterior segment manifestations in the NS group and 5-day after surgery of control and Grx1 KO mice. (B) GSH/GSSG ratio of control and Grx1 KO mice measured in the NS group and 5 days after surgery. (C) Immunofluorescence staining of control and Grx1 KO mice lens capsules for the NS group and 5 days after surgery. Nuclei were counterstained with DAPI (blue). Pro-SSG presented as green, fluorescent light. (D) Immunofluorescence staining of control and Grx1 KO mice lens capsules for the NS group and 5 days after surgery. Nuclei were counterstained with DAPI (blue), vimentin presented as green, fluorescent light and α-SMA presented as red, fluorescent light. (E) Western blotting indicating α-SMA and vimentin protein levels for the NS groups and 5 days after surgery in control and Grx1 KO mice. Columns represent the mean ± SEM, n = 3, *P < 0.05, **P < 0.01, ***P < 0.001.

from the preview scan in the Orbitrap. The raw MS files were analyzed and searched against the target protein database based on the species of the samples using MaxQuant (1.6.2.10). The parameters were set as follows: the protein modifications were carbamidomethylation (C) (variable), oxidation (M) (variable), acetylation (Protein N-term) (variable), and S-glutathionylation (C) (variable); the enzyme specificity was set to trypsin. The maximum missed cleavages were set to two; the precursor ion mass tolerance was set to 20 ppm, and MS/MS tolerance was 20 ppm. Only highly confident identified peptides were chosen for downstream protein identification analysis. From the determination of protein concentration to analysis the data were done by Biotech pack scientific Co., Ltd.

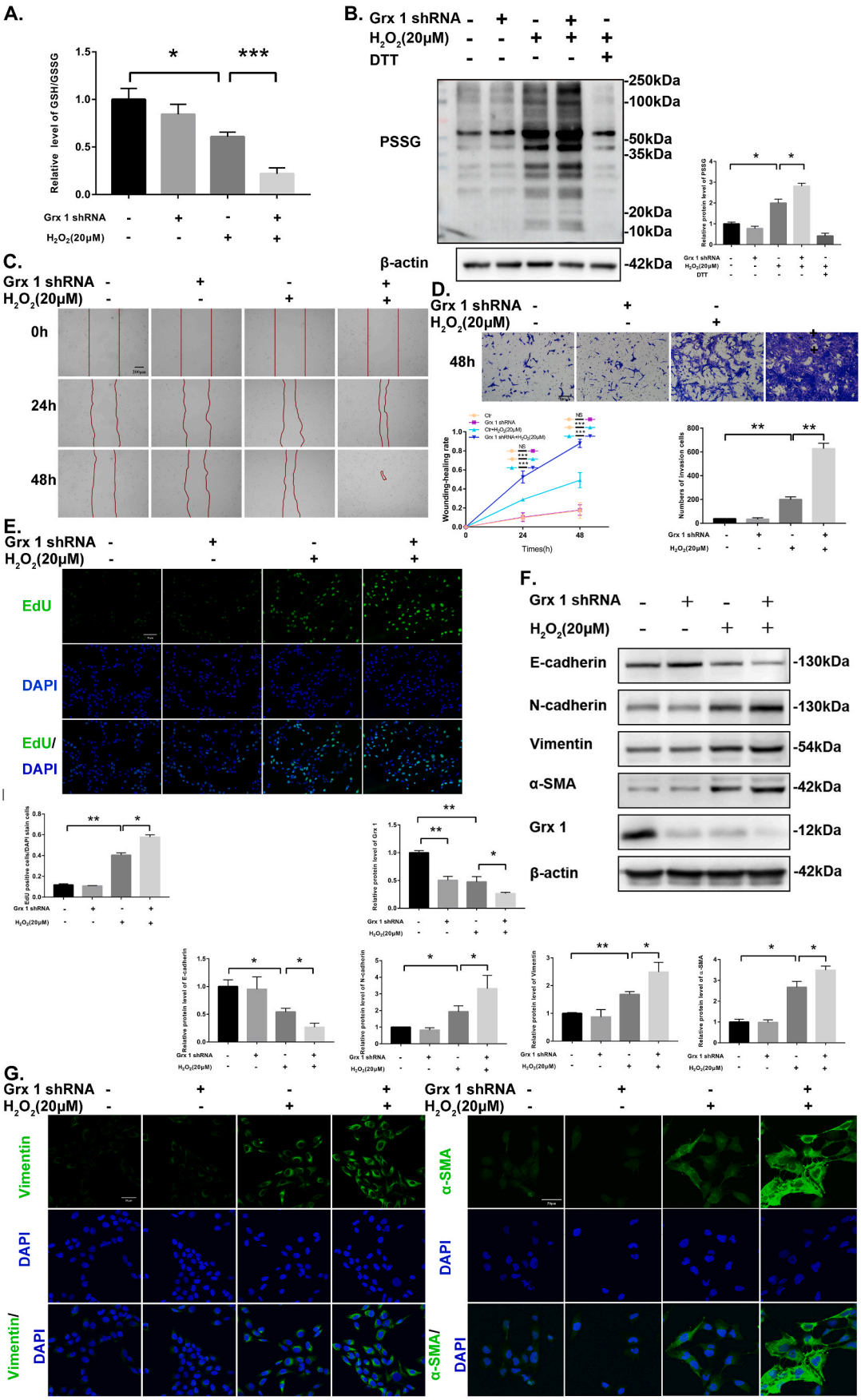

(caption on next page)

Fig. 3. Knockdown of Grx1 upregulated H_2O_2 induced S-glutathionylation and EMT in LECs.
H_2O_2-treated (20 μM for 24 h) and untreated LECs were transfected with control shRNA or Grx1 mRNA-targeting shRNA. (A) DTNB assay of GSH/GSSG ratios. (B) Western blotting indicating protein S-glutathionylation levels under non-reducing conditions with anti-GSH antibody. (C) Wound healing assay showing cell migration at 0 h, 24 h, and 48 h. (D) Transwell migration results expressed as the number of migrated cells. (E) EdU staining assay (green) results expressing cell proliferation. (F) Western blotting detection of EMT protein markers (vimentin, α-SMA, and N-cadherin) and epithelial cell protein markers (E-cadherin). (G) Immunofluorescence staining of vimentin (green) and α-SMA (green). Nuclei were counterstained with DAPI (blue). Columns represent the mean ± SEM, n = 3, *P < 0.05, **P < 0.01, ***P < 0.001.

2.12. Detection of protein S-glutathionylation

After washing three times with ice-cold PBS, the cells were lysed and extracted using a Pierce Classic Magnetic IP/Co-IP Kit (Thermo Scientific, 88804) according to the manufacturer's protocol. The samples were incubated (overnight, 4 °C) with anti-glutathione (Abcam, ab19534, 1:200) antibodies whereafter Co-IP was conducted on a magnetic rack (Thermo Scientific) according to the manufacturer's protocol. The samples were analyzed by Western blotting.

2.13. Detection of S-glutathionylated CK1α in vitro purification experiment [24]

In total, 2 μg recombinant human CK1α protein (Sino Biological, 10668-H09B) was incubated with 1 mM GSSG (Sigma, G6654) or 250 μM GSH (Sigma, G4251) plus 250 μM H_2O_2 for 15 min, then mixed with Grx1 redox system, including 13.5 μg/mL recombinant human Grx1 (Sino Biological, 14484-H07E), 35 μg/mL GSSG reductase (Sigma, G3664), 1 mM GSH, 18 μM EDTA (Sigma, E6758), 1 mM NADPH (Beyotime, S0053-6), 137 mM pH 8.0 Tris-HCl (Beyotime, ST788) or 50 mM DTT (Sigma, DTT-RO) for 30 min. Samples were analyzed via Western blotting with anti-GSH antibody under non-reducing conditions.

2.14. In vitro kinase activity assay [33]

0.2 μg recombinant human CK1α protein (Sino Biological, 10668-H09B) was incubated as above-mentioned. 2 μg recombinant human β-catenin (Sino Biological, 11279-H20B), 200 μM ATP (Cell Signaling, #9804), and kinase buffer were incubated for 20 min at 23 °C. Phosphorylation of β-catenin Ser45 was detected by Western blotting using phospho-specific antibody (Cell Signaling, 9564S). Kinase buffer was prepared from 25 mM pH 7.5 HEPES (Solarbio, H1095), 100 mM NaCl (Solarbio, S8210), 10 mM $MgCl_2$ (Solarbio, M8161), 5% glycerol (Solarbio, G8190), 0.1% NP-40 (Solarbio, N8030).

2.15. Statistical analysis

Statistical Product and Service Solutions 19.0 software (IBM SPSS) was used for statistical analyses. All data are presented as the mean ± standard error of the mean for at least three independent experiments. In addition, the means of three or more groups were compared using a *t*-test and one-way analysis of variance. Statistical significance was set at P-value<0.05.

3. Results

3.1. Downregulation of Grx1 expression following cataract surgery in mice and increased PCO susceptibility in Grx1 KO mice

To confirm the role of Grx1 in PCO, mice were subjected to cataract surgery *in vivo* experiments. To ensure the reproducibility of human LECs, HLE-B3 cells were used *in vitro* experiments, and LECs were treated with H_2O_2, which reportedly induces EMT [17,18]. HE staining of the *bulbus oculi* showed non-surgery (NS) and post-surgery capsular manifestations. As shown in Fig. 1A, we removed the cortex and nucleus of lens to simulate post-cataract surgery environment. After cataract surgery, we could observe residual cells in anterior and equatorial capsules, wherein posterior capsules were transparent. Interestingly, capsular Grx1 expression was downregulated compared to that in NS capsules (Fig. 1B). We further detected Grx1, α-SMA, and vimentin expressions at the mRNA and protein levels both *in vivo* and *in vitro* experiments. *In vivo* experiments, the mRNA level of α-SMA increased 1, 3 and 5 days after surgery. vimentin increased 3 and 5 days after surgery, and Grx1 increased 1, 3 and 5 days after surgery compared to that seen with NS group (Fig. 1C). Although the increase in the protein levels of α-SMA and vimentin was consistent with their transcript level, Grx1 expression was conversely decreased 1, 3 and 5 days after surgery compared to seen with NS expression (Fig. 1D). We further performed *in vitro* experiments. *In vitro* experiments, mRNA level of α-SMA increased after 12 h, 24 h, and 48 h, vimentin increased after 24 h and 48 h, and Grx1 expression increased 6 h, 12 h, 24 h, and 48 h after H_2O_2 treatment (Fig. 1E). The increases in the protein levels of α-SMA and vimentin were also consistent with their transcript levels *in vitro* experiments. However, the protein level of Grx1 increased 6 h and 12 h after H_2O_2 treatment and then decreased after 24 h and 48 h (Fig. 1F). We found differential Grx1 expression at different times *in vivo* and *in vitro* experiments. Moreover, both *in vivo* and *in vitro* experiments concurred that the protein expression level of Grx1 negatively correlates with the expression of EMT marker proteins. This may indicate the mechanistic importance of Grx1 in PCO development.

Accordingly, we engineered Grx1 KO mice for further experiments. We detected the mRNA expression profile of Grx1, Grx2, and thioredoxin 1 (Trx1) at lens capsule, retina, and lung. The results showed Grx1 was absent in Grx1 KO mice, whether Grx2 and Trx1 did not differ between Grx1 KO and control mice (Fig. S1). HE staining of the *bulbus oculi* showed that Grx1 KO mice developed more severe PCO after cataract surgery than control mice (Fig. 2A). In Grx1 KO mice, cells proliferated and migrated from the anterior to the posterior capsule, and a large number of cells accumulated in the central posterior capsule. Conversely, the central posterior capsule of control mice was nearly transparent. Additionally, the GSH/GSSG ratio, which provides a reliable estimate of the cellular redox status, was lower in the lens capsules of the surgery group than in the NS group. Moreover, the GSH/GSSG ratio in Grx1 KO mice decreased more than in the surgery group control mice (Fig. 2B). We further measured the level of protein S-glutathionylation in the capsules using anti-GSH antibody by immunofluorescence staining. Predictably, this protein S-glutathionylation was higher in the Grx1 KO mice than in the control mice and NS group (Fig. 2C). Correspondingly, Western blotting and immunofluorescence staining showed that vimentin and α-SMA expression were upregulated in the Grx1 KO mice residual lens posterior capsules compared to that in the control and NS group mice (Fig. 2D and E). Overall, Grx1 expression was downregulated in mice following cataract surgery. The resultant reduced Grx1 levels may subsequently mediate the upregulation of S-glutathionylation and EMT, participating in the occurrence of PCO *in vivo* and *in vitro*.

3.2. Knockdown of Grx1 upregulated H_2O_2-induced S-glutathionylation and EMT in LECs

To further investigate the role of Grx1 in S-glutathionylation and EMT of LECs, lentivirus-mediated knockdown of Grx1 was performed. HLE-B3 cells were transfected with control LVCON207 or three different types of LV-Grx1-RNAi (45698-1, 57933-1, and 52211-1). All lentiviruses were labeled with fluorescent fragments. Subsequent fluorescence

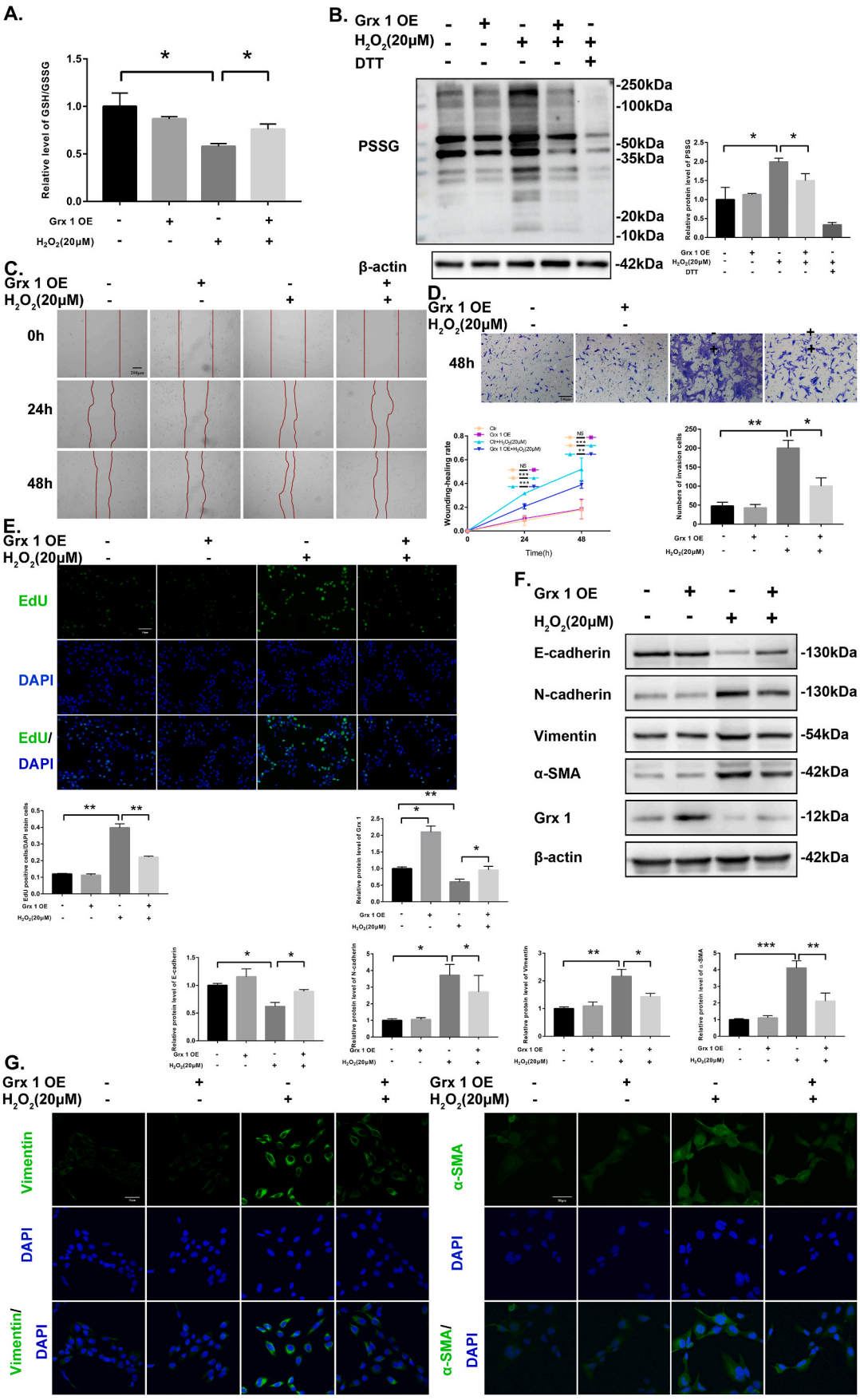

(caption on next page)

Fig. 4. Overexpression of Grx1 downregulated H_2O_2-induced S-glutathionylation and EMT in LECs.
H_2O_2-treated (20 μM for 24 h) and untreated LECs were transfected with control or Grx1 overexpression RNA. (A) DTNB measurements of GSH/GSSG ratios. (B) Western blotting indicating protein S-glutathionylation levels under non-reducing conditions with anti-GSH antibody. (C) Wound-healing assay showing cell migration at 0 h, 24 h, and 48 h. (D) Transwell migration results expressed as the number of migrated cells. (E) EdU staining assay (green) expressing cellular proliferation. (F) Western blotting indicating EMT protein marker (vimentin, α-SMA, and N-cadherin) and epithelial cell protein marker (E-cadherin) levels. (G) Immunofluorescence staining of vimentin (green) and α-SMA (green). Nuclei were counterstained with DAPI (blue). Columns represent the mean ± SEM, n = 3, *P < 0.05, **P < 0.01, ***P < 0.001.

microscopy showed that both control and LV-Grx1-RNAi were successfully transfected into cells (Fig. S2A). Grx1 knockdown efficiency was determined by qPCR following cDNA extraction. The Grx1 knockdown efficiency of LV-Grx1-RNAi-52211-1 was the highest among the LV-Grx1-RNAi types (Fig. S2B). Moreover, Western blotting analysis showed that Grx1 expression decreased by as much as 50% in LV-Grx1-RNAi-52211-1 compared to control (Fig. S2C). Therefore, we used LV-Grx1-RNAi-52211-1 (shRNA) for subsequent functional analyses.

To confirm the function of Grx1-regulated S-glutathionylation in LECs, GSH/GSSG ratios and protein S-glutathionylation levels were evaluated. Grx1 knockdown and H_2O_2 co-treatment decreased GSH/GSSG ratios and increased protein S-glutathionylation levels compared with the single H_2O_2 treatment group (Fig. 3A and B). We further detected the EMT phenotypes of LECs using wound healing, transwell migration, and EdU staining assays. Compared with H_2O_2-treated LECs, Grx1 knockdown and H_2O_2 co-treatment promoted LEC migration (Fig. 3C and D). The proliferative ability of LECs was assessed using EdU staining assays. The percentage of proliferating cells in the Grx1 knockdown and H_2O_2 co-treatment group was significantly higher than that in the single H_2O_2 treatment group (Fig. 3E).

Additionally, the Western blotting results suggested that H_2O_2 induced increased expression of EMT protein markers, including vimentin, α-SMA, and N-cadherin, in LECs. Moreover, Grx1 knockdown and H_2O_2 co-treatment increased the expression of these EMT protein markers compared to that in the single H_2O_2 treatment group. Conversely, the expression of E-cadherin, a protein marker of epithelial cells, showed an opposite trend to that of the aforementioned proteins (Fig. 3F). Immunofluorescence staining further confirmed the Western blotting results (Fig. 3G). These results indicate that Grx1 knockdown aggravated oxidative stress, consequentially increased S-glutathionylation level, and upregulated EMT in LECs.

3.3. Overexpression of Grx1 downregulated H_2O_2-induced S-glutathionylation and EMT in LECs

Lentivirus-mediated Grx1 overexpression in LECs was used to investigate whether H_2O_2-induced EMT could be reversed. Accordingly, LECs were successfully transfected with control LVCON294 and LV-Grx1-74528-2, indicated using fluorescence microscopy, qPCR and Western blotting showed that the mRNA and protein expression levels of Grx1 increased (Figs. S2D–F) in LV-Grx1-74528-2 transfected LECs compared to that of the control; therefore, LV-Grx1-74528-2 was used for subsequent functional analyses.

Grx1 overexpression and H_2O_2 co-treatment increased GSH/GSSG and decreased protein S-glutathionylation levels compared with those of the single H_2O_2 treatment group (Fig. 4A and B). Compared with the EMT phenotype of LECs treated with H_2O_2, Grx1 overexpression and H_2O_2 co-treatment inhibited cellular migration and decreased the number of migrated cells (Fig. 4C and D). Moreover, Grx1 overexpression co-treated with H_2O_2 exhibited a significantly lower cellular proliferation percentage than the single H_2O_2 treatment group (Fig. 4E).

Correspondingly, vimentin, α-SMA, and N-cadherin expression in the Grx1 overexpression co-treated with the H_2O_2 group decreased compared to those in the single H_2O_2 treatment group. However, E-cadherin expression was in contrast to that of the aforementioned proteins (Fig. 4F). Immunofluorescence staining further confirmed the Western blotting results (Fig. 4G). In summary, these results suggest that Grx1 is involved in the regulation of redox status and S-glutathionylation, thereby affecting EMT in LECs.

3.4. LC-MS/MS analysis of H_2O_2-induced cysteine S-glutathionylation in LECs

After establishing that Grx1 could regulate protein S-glutathionylation, which plays a vital role in PCO formation, we aimed to identify the specific molecular targets and pathways susceptible to redox-dependent regulation in the pathogenesis of PCO. This was achieved *via* LC-MS/MS analysis of protein S-glutathionylation levels in H_2O_2-treated and untreated LECs (Fig. 5A). LC-MS/MS results that were reproducible over three repetitions were selected for subsequent a large number of document retrieval, thereby selected GSK-3β, CK1α (CSNK1A1), DSTN, and axin 1 correlating with EMT for further study. In addition, S-glutathionylation levels in H_2O_2-treated and untreated LECs were evaluated by Co-IP using an anti-GSH antibody. CK1α-SSG levels were higher in H_2O_2-treated LECs than in control; however, the other proteins were not detected (Fig. 5B). Therefore, we selected CK1α as the molecular target for further exploration.

3.5. Grx1 could regulate S-glutathionylation and the activity of CK1α

Studies have demonstrated that CK1α phosphorylates β-catenin at Ser45, which leads to the subsequent degradation of β-catenin, thereby decreasing its nuclear translocation. Moreover, CK1α is an essential negative regulator of the Wnt/β-catenin signaling pathway [30]. Using

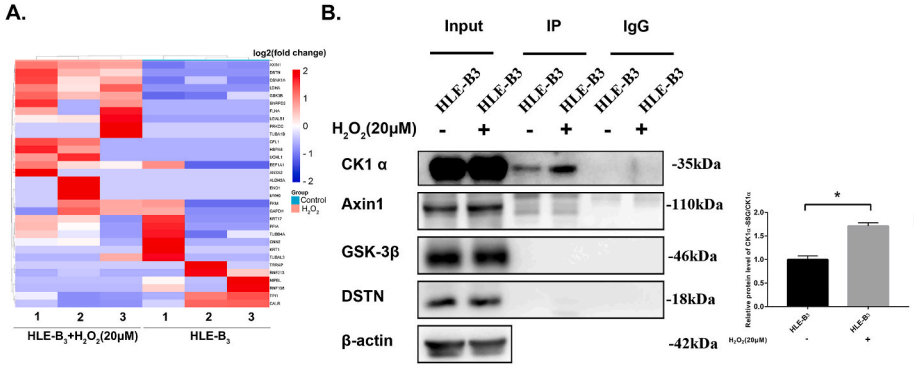

Fig. 5. LC–MS/MS analysis of H_2O_2-induced cysteine S-glutathionylation in LECs.
Comparative groups include H_2O_2-treated (20 μM for 24 h) and untreated LECs. (A) The heatmap of LC-MS/MS results indicates protein S-glutathionylation levels of comparative groups. (B) LC-MS/MS and a large number of document retrieval results of GSK-3β, CK1α, DSTN, and axin 1 S-glutathionylation levels were evaluated via Co-IP using an anti-GSH antibody. Columns represent the mean ± SEM, n = 3, *P < 0.05, **P < 0.01, ***P < 0.001.

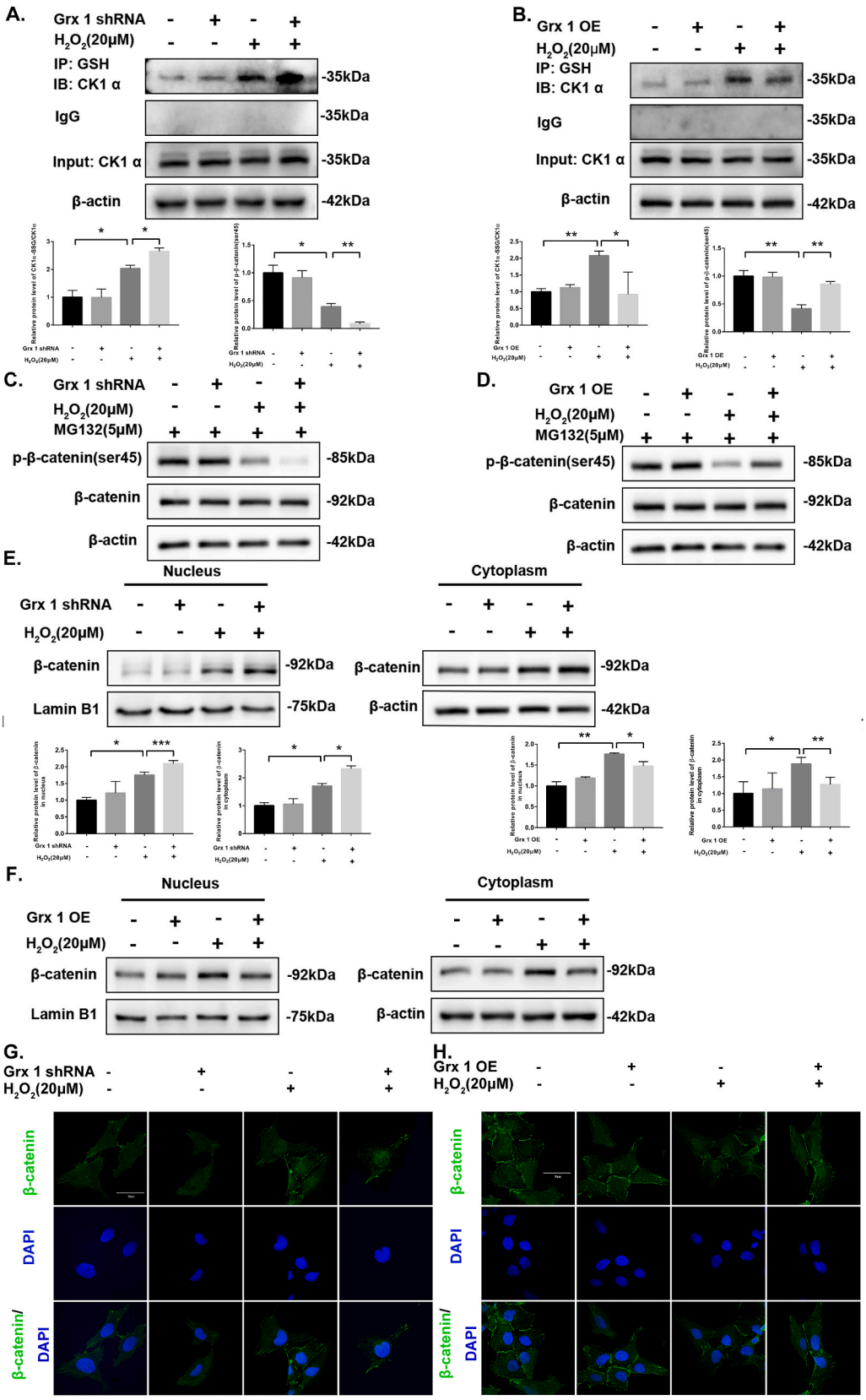

Fig. 6. Grx1 could regulate S-glutathionylation and the activity of CK1α.
H_2O_2-treated (20 μM for 24 h) and untreated LECs were transfected with control shRNA, shRNA targeting Grx1 mRNA, control RNA, or Grx1 overexpression RNA. (A and B) S-glutathionylation of CK1α was evaluated using Co-IP with an anti-GSH antibody. (C and D) Western blotting indicating phospho-β-catenin (Ser45) levels which proteasomal inhibitor MG132 was used to make similar levels of β-catenin. (E and F) Western blotting showing the expression of β-catenin in both the nucleus and cytoplasm. (G and H) Immunofluorescence staining was used to detect the nuclear translocation of β-catenin (green). Nuclei were counterstained with DAPI (blue). Columns represent the mean ± SEM, n = 3, *P < 0.05, **P < 0.01, ***P < 0.001.

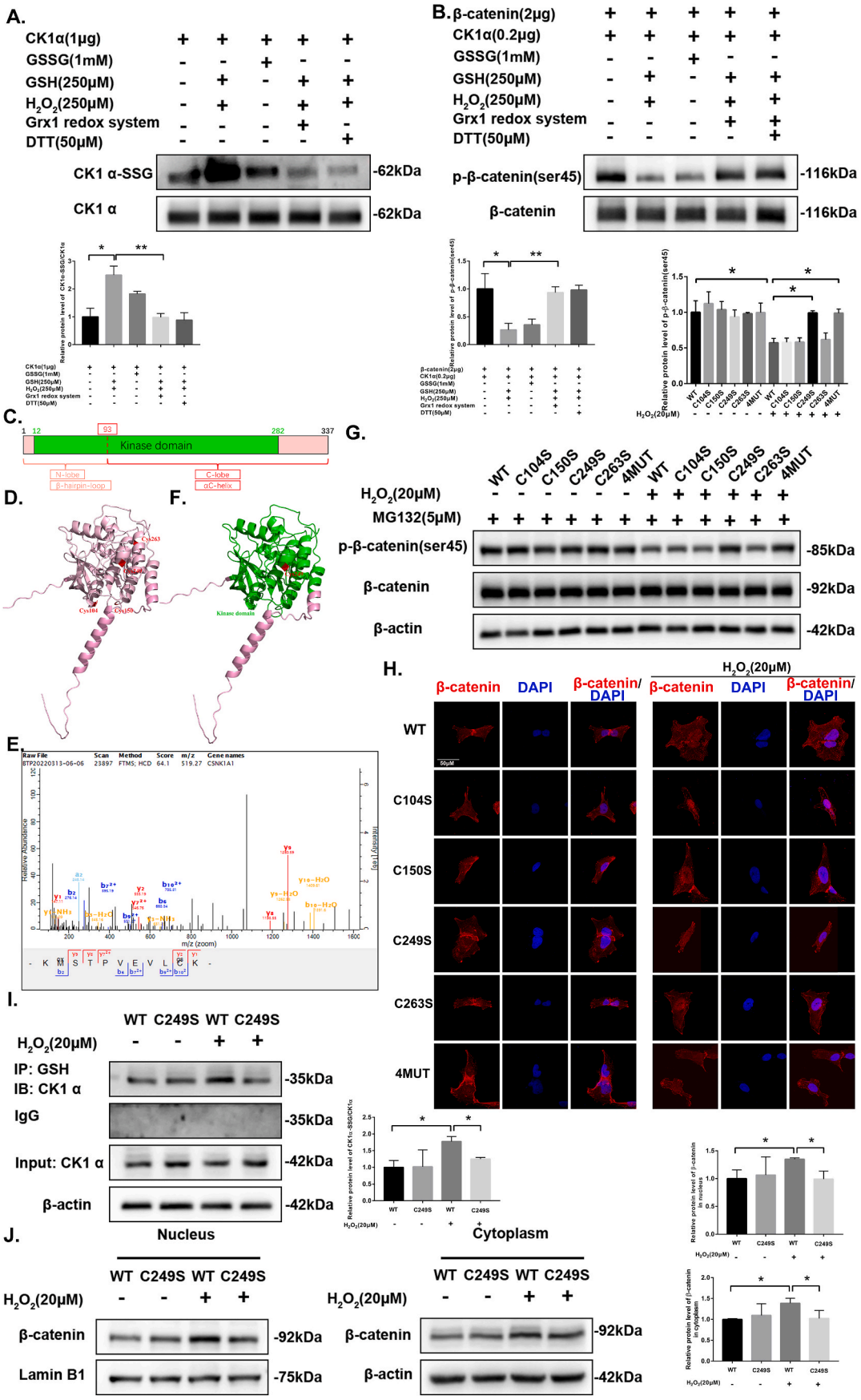

(caption on next page)

Fig. 7. Cys249 S-glutathionylation inhibited the function of CK1α.
(A) Purified recombinant protein CK1α was incubated with GSH plus H_2O_2 or GSSG for 15 min and then mixed with- Grx1 redox system or DTT for 30 min. Western blotting indicating protein S-glutathionylation levels under non-reducing conditions with anti-GSH antibody. (B) After incubation in different redox states, CK1α was incubated with purified β-catenin and ATP for 23 min. Western blotting indicating phospho-β-catenin (Ser45) levels. (C) Representation of CK1α domain by color and boundaries. (D) Model structure of CK1α and its four cysteines, generated by Pymol based on the crystal structure of Homo sapiens CK1α (AlphaFold ID, AF-P48729-F1). (E) Mass spectra of a CK1α peptide glutathionylated at Cys249. (F) Model structure of CK1α and its kinase domain, generated by Pymol based on the crystal structure of CK1α (AlphaFold ID, AF-P48729-F1). H_2O_2-treated (20 μM for 24 h) and untreated LECs were transfected with WT, C104S, C150S, C249S, C263S, and 4MUT CK1α. (G) Western blotting indicating phospho-β-catenin (Ser45) levels which proteasomal inhibitor MG132 was used to make similar levels of β-catenin. (H) Immunofluorescence staining detected the nuclear translocation of β-catenin (red). Nuclei were counterstained with DAPI (blue). H_2O_2-treated (20 μM for 24 h) and untreated LECs were transfected with WT or C249S CK1α. (I) CK1α S-glutathionylation levels were evaluated via Co-IP using an anti-GSH antibody. (J) Western blotting indicating the expression of both nuclear and cytoplasmic β-catenin. Columns represent the mean ± SEM, n = 3, *P < 0.05, **P < 0.01***, P < 0.001.

Co-IP with an anti-GSH antibody, we detected the highest CK1α-SSG levels in the Grx1 knockdown co-treated with H_2O_2 group, followed by that of the single H_2O_2 treatment group finally, a somewhat reversed CK1α-SSG in the Grx1 overexpression co-treated with H_2O_2 group (Fig. 6A and B). This indicated that CK1α is susceptible to S-glutathionylation and can be regulated by varying Grx1 levels. Next, we investigated whether S-glutathionylation influenced the phosphorylation of β-catenin at Ser45. We used proteasomal inhibitor MG132 (Selleck, S2619) to make similar levels of β-catenin and compared the phosphorylation levels. Accordingly, Ser45 levels decreased after H_2O_2 treatment, a result that was aggravated by Grx1 knockdown and reversed by Grx1 overexpression (Fig. 6C and D). We then evaluated the nuclear and cytoplasmic β-catenin levels via Western blotting. These results suggested that the expression of both nuclear and cytoplasmic β-catenin levels increased in the Grx1 knockdown co-treated with H_2O_2 group and decreased in the Grx1 overexpression co-treated with H_2O_2 group compared to that in the single H_2O_2 treatment group (Fig. 6E and F). Immunofluorescence staining confirmed this nuclear translocation of β-catenin (Fig. 6G and H). These results indicate that Grx1 can regulate S-glutathionylation and the activity of CK1α. Moreover, CK1α-SSG may inhibit the phosphorylation of β-catenin at Ser45 and increase the nuclear translocation of β-catenin. We further detected the glutathionylation level of CK1α *in vitro* purification experiments. As shown in Fig. 7A, GSSG or GSH plus H_2O_2 could increase level of CK1α-SSG, which Grx1 could reverse it. *In vitro* kinase activity assay, GSSG or GSH plus H_2O_2 could decrease phosphorylation of β-catenin at Ser45 levels, indicating decreased activity of CK1α, which Grx1 could reverse (Fig. 7B).

3.6. Cys249 S-glutathionylation inhibited the function of CK1α

CK1α comprises 337 amino acids, with a kinase domain located between Ile12 and Ala282 [34]. Its 2.45 Å crystal structure revealed that the first 93 amino acids form a β-hairpin loop [35,36]. The C-lobe of CK1α is mainly composed of αC helices that contribute to its kinase function (Fig. 7C) [30]. *Homo sapiens* CK1α has four cysteines: Cys104, Cys150, Cys249, and Cys263 (Fig. 7D). Notably, LC-MS/MS analysis showed that Cys249, which is located in the kinase domain, was the S-glutathionylation site of CK1α (Fig. 7E and F).

To determine whether Cys249 regulates CK1α, we constructed WT, C104S, C150S, C249S, C263S, 4MUT CK1α and assayed their activity individually. Fluorescence microscopy showed that all RNA types were successfully transfected into LECs (Fig. S3A). The overexpression efficiency of WT and cysteine mutant CK1α in the LECs was determined by qPCR and Western blotting (Figs. S3B and C). As Fig. 7G shown, C249S and 4MUT could reverse decreased phosphorylation level of β-catenin at Ser45 under H_2O_2 treatment. Immunofluorescence staining also implied that C249S and 4MUT could reverse the nuclear translocation of β-catenin under H_2O_2 treatment (Fig. 7H). According to the results of LC-MS/MS analysis, fluorescence microscopy, and Western blotting, we speculated that Cys249 S-glutathionylation inhibited the function of CK1α. Furthermore, S-glutathionylation levels were evaluated using Co-IP with an anti-GSH antibody. H_2O_2 treatment increased WT CK1α-SSG, whereas C249S blocked this H_2O_2-induced increase (Fig. 7I). Concurrently, H_2O_2 treatment increased nuclear accumulation of β-catenin in the WT group, this effect was blocked by C249S (Fig. 7J).

3.7. Cys249 S-glutathionylation was critical for H_2O_2-induced EMT in LECs

We further examined the H_2O_2-induced EMT phenotypes of WT and C249S LECs. C249S markedly attenuated the H_2O_2-induced increase in cellular migration and proliferation (Fig. 8A–C). Additionally, the H_2O_2-induced increases in vimentin, α-SMA, and N-cadherin expression in the WT group was blocked in the C249S group. The change in E-cadherin expression was opposite to that of the aforementioned proteins (Fig. 8D). Immunofluorescence staining further confirmed these results (Fig. 8E). In summary, CK1α-SSG at Cys249 inhibited the phosphorylation of β-catenin at Ser45, promoted the nuclear translocation of β-catenin, and aggravated EMT in LECs.

4. Discussion

The outer fiber layer of the lens is a GSH-enriched zone (>10 mM) [37] as opposed to the aqueous humor (~5 μM) [16]. Cataract surgery directly exposes LECs to the aqueous humor, markedly reducing their antioxidant capacity [16], and leading to oxidative stress. Our previous *in vitro* and *in vivo* models suggested that oxidative stress activates the Wnt/β-catenin signaling pathway, resulting in EMT of LECs and the occurrence of PCO [17,18]. Oxidative stress has been confirmed to drive S-glutathionylation of proteins [19] which can regulate the structure and function of target protein [20–24]. For example, the S-glutathionylation of GAPDH [38], rac-1 [39], AKT [20], estrogen receptor alpha [40], catalase [41] and sirtuin-1 [21] inhibits protein function. Conversely, S-glutathionylation of AMPK [42], actin [43], mitofusin [22] and FABP5 [24] activates protein function. Grx1 is a cytoplasmic enzyme that maintains a reducing environment by catalyzing protein deglutathionylation, and has been implicated in the pathogenesis of many diseases [24–28]. Grx1 performs a wide range of antioxidant functions in the lens and prevents protein-thiol mixed disulfide accumulation reducing the protein–protein aggregation, insolubilization, and apoptosis of LECs [29]. However, whether Grx1-regulated protein S-glutathionylation plays an essential role in PCO remains unclear. In this study, we revealed that Grx1 expression was downregulated in mice following cataract surgery, and Grx1 KO mice developed more severe PCO than the control. Additionally, Grx1 knockdown aggravated S-glutathionylation and EMT of LECs, which could be reversed by Grx1 overexpression under oxidative stress. According to LC-MS/MS and further exploration, S-glutathionylation at Cys249 of CK1α inhibited its phosphorylating activity at Ser45 of β-catenin, thereby promoting the nuclear translocation of β-catenin and aggravating EMT of LECs.

Our study is the first to report that protein level of Grx1 is downregulated in mice after cataract surgery. Similarly, Guo et al. [24] found that hyperoxia significantly decreased Grx1 expression in an acute lung injury model. Interestingly, we found that, at the same time, the mRNA of Grx1 is inconsistent with the protein level in our study. And Lou et al. [44] reported an H_2O_2-induced (100 μM) transient increase and gradual decrease in Grx1 mRNA in LECs. Studies also shown the activation and

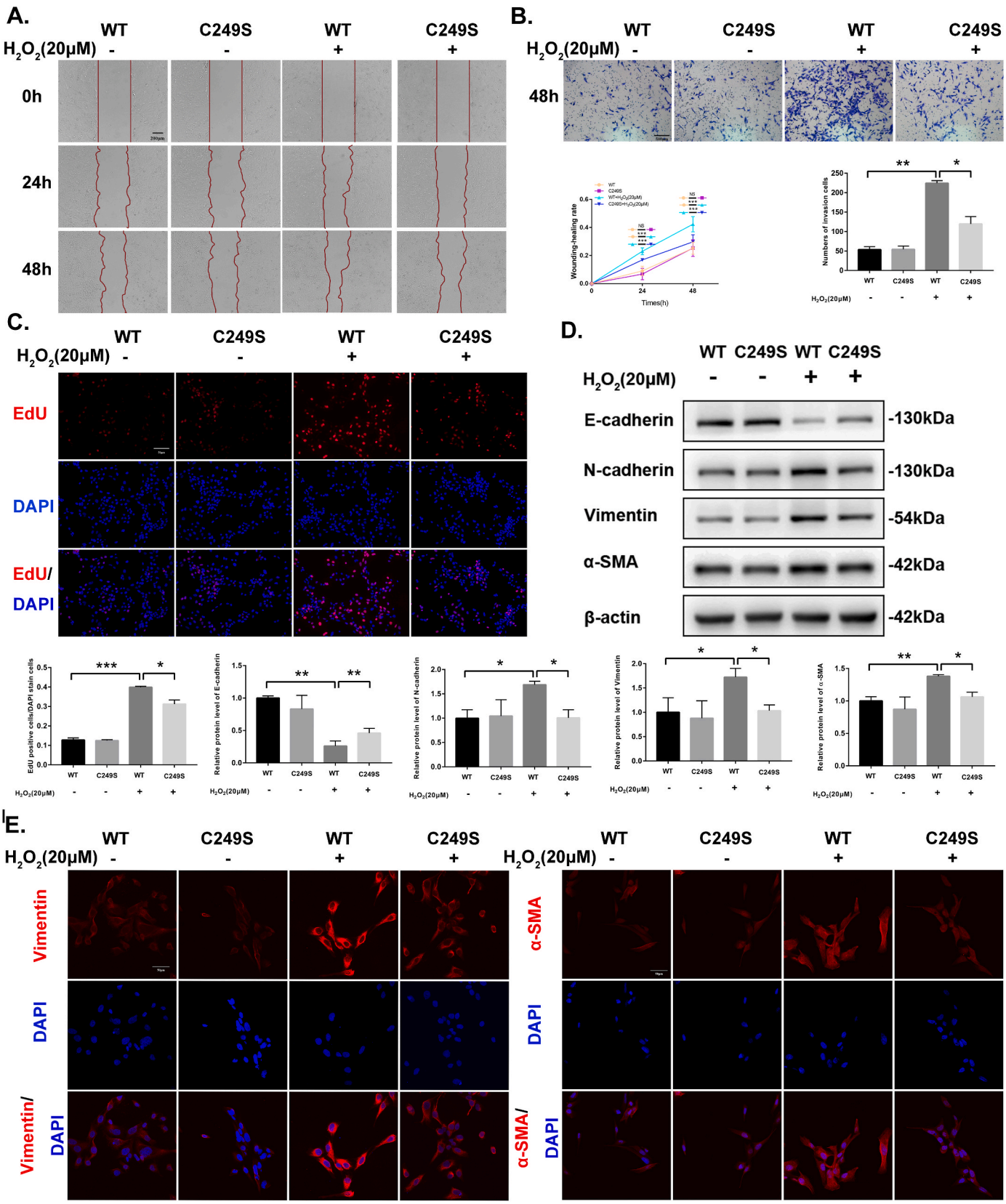

Fig. 8. Cys249 S-glutathionylation was critical for H_2O_2-induced EMT in LECs.
H_2O_2-treated (20 μM for 24 h) and untreated LECs were transfected with WT or C249S CK1α. (A) Wound healing assay showing cell migration at 0 h, 24 h, and 48 h. (B) Transwell migration results were expressed as the number of migrated cells. (C) EdU staining assay (red) was used to detect proliferating cells. (D) Western blotting indicating EMT protein marker (vimentin, α-SMA, and N-cadherin) and epithelial cell protein marker (E-cadherin) levels. (E) Immunofluorescence staining results indicating the protein expression levels of vimentin (red) and α-SMA (red). Nuclei were counterstained with DAPI (blue). Columns represent the mean ± SEM, n = 3, *P < 0.05, **P < 0.01, ***P < 0.001.

inactivation of Grx1 may also be related to the AP-1 transcription factor [45] and GSH/GSSG ratio [46]. So, we speculated that the mRNA level change may related to the H_2O_2 treatment concentrations, representing the oxidative stress level. And sustained high H_2O_2 treatment concentrations would damage the capacity of transcription. Furthermore, the inconsistent between mRNA and protein level indicated that the downregulated expression of Grx1 might exist in regulation in the translation process, which requires further study.

In general, loss of Grx1 leads to a perturbed cytosolic redox state, increased protein S-glutathionylation levels, and disrupted redox signaling [19]. Additionally, we demonstrated that Grx1 regulates S-glutathionylation and the GSH/GSSG ratio. Grx1 knockdown decreased the GSH/GSSG ratio and increased protein S-glutathionylation, whereas Grx1 overexpression reversed this effect. Similarly, LöFgren et al. [47] confirmed that a Grx1 deficiency in LECs decreases GSH levels and resistance to oxidative stress, and elevates protein S-glutathionylation. Firstly, we found Grx1 knockdown upregulated the proliferation, migration, and EMT marker expression of LECs following H_2O_2-induced EMT, which could be reversed by Grx1 overexpression. The findings of Lee. et al. [48] closely resembled ours in that Grx1 expression was negatively correlated with the level of EMT in EpRas mammary epithelial cells. We further explored the mechanism by which Grx1 regulates EMT, which is highly significant in treating PCO.

LC-MS/MS was used to analyze protein S-glutathionylation levels under oxidative conditions to identify the specific molecular targets. Notably, a previously reported S-glutathionylation site of GAPDH [38] was identified in our analyses, providing additional support to our results. Our previous study showed that the TGF-β and Wnt/β-catenin signaling pathways were activated during PCO formation [18]. However, Wei et al. [17] suggested that decreased GSH triggered the Wnt/β-catenin signaling pathway independent of TGF-β during lens fibrosis and PCO formation via EMT-mediated mechanisms. These results suggest that Grx1 and S-glutathionylation may be related to the activation of Wnt/β-catenin signaling pathways under oxidative stress. Correspondingly, we first discovered that CK1α-SSG inhibits kinase activity and promotes activation of Wnt/β-catenin signaling in EMT of LECs under oxidative stress.

CK1α is an essential negative regulator of Wnt/β-catenin signaling [30]. CK1α phosphorylates β-catenin at Ser45 as part of the β-catenin destruction complex, leading to its subsequent degradation [31]. Recent studies have found that CK1α activity may be linked to its phosphorylation at Thr321 [49], miR-155 and miR -9-5p [50–52] at post-transcriptional level, ATP-dependent RNA helicase-DDX3 [53]. In our study, to determine which site of cysteine plays a significant role in the regulation of CK1α, we mutated cysteine to serine and compared its activity with that of WT CK1α. The results showed that C249S blocked the H_2O_2-induced decrease in β-catenin phosphorylation and nuclear translocation, inhibiting EMT. Our study first discovered that Cys249 is an important S-glutathionylation site, which regulates the activity of CK1α.

Notably, the Wnt/β-catenin signaling pathway, for which CK1α acts as a negative regulator, is an attractive target for disease treatment. Clarifying the underlying mechanisms of the activation/inactivation of CK1α is of great significance and could provide a basis for designing highly targeted and more effective drugs. Whether CK1α-SSG inhibits CK1α activity and promotes EMT in other diseases should be considered in further studies. Grx1 plays a regulatory role in PCO, and its overexpression inhibits the EMT of LECs by catalyzing deglutathionylation of CK1α and recovering kinase activity. These results indicate the potential of Grx1 as a chemotherapeutic target. Exogenous administration of recombinant Grx1 reversed the increase in PSSG induced by lung fibrosis [54]. For the treatment of PCO, a multidisciplinary team should manage the administration methods, doses, and dosage forms.

The limitations of this study are as follows. First, Grx1 expression, and associated thiol redox function have been reported to be sexual dimorphism, according to recent studies [55,56]. In PCO, several epidemiological studies have suggested that women have a significantly higher risk than men [57–59], although other studies do not support this correlation [60]. In our study, the experimental mice of both genders were mixed for all the experiments. And whether the effect of Grx1 exists sexual dimorphism needs further investigation. Secondly, TGF-β signal pathway plays a vital role in PCO; whether TGF-β-treated could result in the differential expression of Grx1 and the effect of Grx1 in TGF-β signal pathway remain unclear. Finally, our LC-MS/MS results showed degradation complex including GSK-3β and Axin1 existed S-glutathionylation, which were not detected by CO-IP. We speculated that the low S-glutathionylation level, the instability modification or the false positive results may cause it. New techniques should be used to explore it precisely. In conclusion, we found that Grx1 expression was downregulated during PCO formation. Reduced Grx1 significantly upregulated S-glutathionylation, increased EMT, and aggravated PCO. Moreover, we further identified that reduced Grx1 expression promoted EMT by upregulating CK1α-SSG under oxidative stress, and that S-glutathionylation at the Cys-249 residue of CK1α inhibited the phosphorylation of β-catenin at Ser45, thereby promoting nuclear translocation of β-catenin and aggravating EMT of LECs. Grx1 and CK1α deglutathionylation may be potential therapeutic targets for PCO.

Funding statement

This work was supported by the National Natural Science Foundation of China (81873674 and 82070947).

Author contributions

C.L., X.C. and H.Y. conceived the project. C.L. and X.C. designed experiments. C.L., X.M., C.L., S.Z and R.Z. performed experiments. C.L. wrote the manuscript. All authors read and approved the final manuscript.

Declaration of competing interest

The authors declare that they have no competing interests.

Data availability

Data will be made available on request.

Acknowledgements

This study was supported by grants from the National Natural Science Foundation of China (81873674 and 82070947). The authors acknowledge the editors and reviewers for their positive and constructive comments and suggestions on our study.

Appendix A. Supplementary data

Supplementary data to this article can be found online at https://doi.org/10.1016/j.redox.2023.102676.

References

[1] C.M. Lee, N.A. Afshari, The global state of cataract blindness, Curr. Opin. Ophthalmol. 28 (1) (2017) 98–103.
[2] Y.-C. Liu, M. Wilkins, T. Kim, et al., Cataracts, The Lancet 390 (10094) (2017) 600–612.
[3] D.A. Schaumberg, M.R. Dana, W.G. Christen, et al., A systematic overview of the incidence of posterior capsule opacification, Ophthalmology 105 (7) (1998) 1213–1221.
[4] B. Li, Y. Wang, M.S. Malvankar-Mehta, et al., Surgical indications, outcomes, and complications with the use of a modified capsular tension ring during cataract surgery, J. Cataract Refract. Surg. 42 (11) (2016) 1642–1648.
[5] A.R. Vasavada, M.R. Praveen, Posterior capsule opacification after phacoemulsification: annual review, Asia Pac. J. Ophthalmol. 3 (4) (2014) 235–240.

[6] J. González-Martín-Moro, J. González-López, F. Gómez-Sanz, et al., Posterior capsule opacification, capsular bag distension syndrome, and anterior capsular phimosis: a retrospective cohort study, Arch. Soc. Esp. Oftalmol. 90 (2) (2015) 69–75.

[7] E. Karahan, D. Er, S. Kaynak, An overview of Nd: YAG laser capsulotomy, Med. Hypothesis, Discov. Innovation (MEHDI) Ophthalmol. 3 (2) (2014) 45.

[8] J. Konopińska, M. Młynarczyk, D.A. Dmuchowska, et al., Posterior capsule opacification: a review of experimental studies, J. Clin. Med. 10 (13) (2021) 2847.

[9] A. Taiyab, J. Holms, J.A. West-Mays, β-Catenin/Smad3 interaction regulates transforming growth factor-β-induced epithelial to mesenchymal transition in the lens, Int. J. Mol. Sci. 20 (9) (2019) 2078.

[10] E. Kubo, T. Shibata, D.P. Singh, et al., Roles of TGF β and FGF signals in the lens: tropomyosin regulation for posterior capsule opacity, Int. J. Mol. Sci. 19 (10) (2018) 3093.

[11] F.J. Lovicu, E. Shin, J.W. Mcavoy, Fibrosis in the lens. Sprouty regulation of TGFβ-signaling prevents lens EMT leading to cataract, Exp. Eye Res. 142 (2016) 92–101.

[12] L.J. Dawes, M.A. Sleeman, I.K. Anderson, et al., TGFβ/Smad4-dependent and-independent regulation of human lens epithelial cells, Invest. Ophthalmol. Vis. Sci. 50 (11) (2009) 5318–5327.

[13] J. Jiang, M.H. Shihan, Y. Wang, et al., Lens epithelial cells initiate an inflammatory response following cataract surgery, Invest. Ophthalmol. Vis. Sci. 59 (12) (2018) 4986–4997.

[14] W. Buehl, O. Findl, T. Neumayer, et al., Short-term changes in the morphology of posterior capsule opacification, J. Cataract Refract. Surg. 31 (5) (2005) 962–968.

[15] T. Neumayer, O. Findl, W. Buehl, et al., Long-term changes in the morphology of posterior capsule opacification, J. Cataract Refract. Surg. 31 (11) (2005) 2120–2128.

[16] J.A. Whitson, D.R. Sell, M.C. Goodman, et al., Evidence of dual mechanisms of glutathione uptake in the rodent lens: a novel role for vitreous humor in lens glutathione homeostasis, Invest. Ophthalmol. Vis. Sci. 57 (8) (2016) 3914–3925.

[17] Z. Wei, J. Caty, J. Whitson, et al., Reduced glutathione level promotes epithelial-mesenchymal transition in lens epithelial cells via a Wnt/β-catenin–mediated pathway: relevance for cataract therapy, Am. J. Pathol. 187 (11) (2017) 2399–2412.

[18] X. Chen, H. Yan, Y. Chen, et al., Moderate oxidative stress promotes epithelial–mesenchymal transition in the lens epithelial cells via the TGF-β/Smad and Wnt/β-catenin pathways, Mol. Cell. Biochem. 476 (3) (2021) 1631–1642.

[19] F.T. Ogata, V. Branco, F.F. Vale, et al., Glutaredoxin: discovery, redox defense and much more, Redox Biol. 43 (2021), 101975.

[20] X. Liu, J. Jann, C. Xavier, et al., Glutaredoxin 1 (Grx1) protects human retinal pigment epithelial cells from oxidative damage by preventing AKT glutathionylation, Invest. Ophthalmol. Vis. Sci. 56 (5) (2015) 2821–2832.

[21] D. Shao, J. Han, X. Hou, et al., Glutaredoxin-1 deficiency causes fatty liver and dyslipidemia by inhibiting sirtuin-1, Antioxid, Redox Signal. 27 (6) (2017) 313–327.

[22] S. Mattie, J. Riemer, J.G. Wideman, et al., A new mitofusin topology places the redox-regulated C terminus in the mitochondrial intermembrane space, J. Cell Biol. 217 (2) (2018) 507–515.

[23] C. Lind, R. Gerdes, I. Schuppe-Koistinen, et al., Studies on the mechanism of oxidative modification of human glyceraldehyde-3-phosphate dehydrogenase by glutathione: catalysis by glutaredoxin, Biochem. Biophys. Res. Commun. 247 (2) (1998) 481–486.

[24] Y. Guo, Y. Liu, S. Zhao, et al., Oxidative stress-induced FABP5 S-glutathionylation protects against acute lung injury by suppressing inflammation in macrophages, Nat. Commun. 12 (1) (2021) 1–18.

[25] M. Burns, S.H.M. Rizvi, Y. Tsukahara, et al., Role of glutaredoxin-1 and glutathionylation in cardiovascular diseases, Int. J. Mol. Sci. 21 (18) (2020) 6803.

[26] O. Gorelenkova Miller, J.J. Mieyal, Sulfhydryl-mediated redox signaling in inflammation: role in neurodegenerative diseases, Arch. Toxicol. 89 (9) (2015) 1439–1467.

[27] A.P. Fernandes, A. Capitanio, M. Selenius, et al., Expression profiles of thioredoxin family proteins in human lung cancer tissue: correlation with proliferation and differentiation, Histopathology 55 (3) (2009) 313–320.

[28] F. Yang, M. Yi, Y. Liu, et al., Glutaredoxin-1 silencing induces cell senescence via p53/p21/p16 signaling axis, J. Proteome Res. 17 (3) (2018) 1091–1100.

[29] M.F. Lou, Glutathione and glutaredoxin in redox regulation and cell signaling of the lens, Antioxidants 11 (10) (2022) 1973.

[30] S. Jiang, M. Zhang, J. Sun, et al., Casein kinase 1α: biological mechanisms and theranostic potential, Cell Commun. Signal. 16 (1) (2018) 1–24.

[31] C. Liu, Y. Li, M. Semenov, et al., Control of β-catenin phosphorylation/degradation by a dual-kinase mechanism, Cell 108 (6) (2002) 837–847.

[32] N. Lois, J. Taylor, A.D. Mckinnon, et al., Posterior capsule opacification in mice, Arch. Ophthalmol. 123 (1) (2005) 71–77.

[33] Q. Huang, L. Chen, E. Schonbrunn, et al., MDMX inhibits casein kinase 1α activity and stimulates Wnt signaling, EMBO J. 39 (14) (2020), e104410.

[34] N. Bidère, V.N. Ngo, J. Lee, et al., Casein kinase 1α governs antigen-receptor-induced NF-κB activation and human lymphoma cell survival, Nature 458 (7234) (2009) 92–96.

[35] J. Krönke, E.C. Fink, P.W. Hollenbach, et al., Lenalidomide induces ubiquitination and degradation of CK1α in del (5q) MDS, Nature 523 (7559) (2015) 183–188.

[36] G. Petzold, E.S. Fischer, N.H. Thomä, Structural basis of lenalidomide-induced CK1α degradation by the CRL4CRBN ubiquitin ligase, Nature 532 (7597) (2016) 127–130.

[37] F.J. Giblin, Glutathione: a vital lens antioxidant, J. Ocul. Pharmacol. Therapeut. 16 (2) (2000) 121–135.

[38] K. Barinova, M. Serebryakova, V. Muronetz, et al., S-glutathionylation of glyceraldehyde-3-phosphate dehydrogenase induces formation of C150-C154 intrasubunit disulfide bond in the active site of the enzyme, Biochim. Biophys. Acta 1861 (12) (2017) 3167–3177.

[39] H. Edenbaum, J. Han, Assessment of S-Glutathionylated Rac1 in cells using biotin-labeled glutathione, Rho GTPases: Methods and Protocols (2018) 155–163.

[40] J. Zhang, Z.-W. Ye, W. Chen, et al., S-Glutathionylation of estrogen receptor α affects dendritic cell function, J. Biol. Chem. 293 (12) (2018) 4366–4380.

[41] S. Nagarkoti, M. Dubey, S. Sadaf, et al., Catalase S-Glutathionylation by NOX2 and mitochondrial-derived ROS adversely affects mice and human neutrophil survival, Inflammation 42 (6) (2019) 2286–2296.

[42] K. Dong, M. Wu, X. Liu, et al., Glutaredoxins concomitant with optimal ROS activate AMPK through S-glutathionylation to improve glucose metabolism in type 2 diabetes, Free Radic. Biol. Med. 101 (2016) 334–347.

[43] R.P. Kommaddi, D.S. Tomar, S. Karunakaran, et al., Glutaredoxin1 diminishes amyloid beta-mediated oxidation of F-actin and reverses cognitive deficits in an Alzheimer's disease mouse model, Antioxid. Redox Signaling 31 (18) (2019) 1321–1338.

[44] N. Raghavachari, K. Krysan, K. Xing, et al., Regulation of thioltransferase expression in human lens epithelial cells, Invest. Ophthalmol. Vis. Sci. 42 (5) (2001) 1002–1008.

[45] K. Krysan, M.F. Lou, Regulation of human thioltransferase (hTTase) gene by AP-1 transcription factor under oxidative stress, Invest. Ophthalmol. Vis. Sci. 43 (6) (2002) 1876–1883.

[46] A.A. Ukuwela, A.I. Bush, A.G. Wedd, et al., Glutaredoxins employ parallel monothiol–dithiol mechanisms to catalyze thiol–disulfide exchanges with protein disulfides, Chem. Sci. 9 (5) (2018) 1173–1183.

[47] S. LöFgren, M.R. Fernando, K.-Y. Xing, et al., Effect of thioltransferase (glutaredoxin) deletion on cellular sensitivity to oxidative stress and cell proliferation in lens epithelial cells of thioltransferase knockout mouse, Invest. Ophthalmol. Vis. Sci. 49 (10) (2008) 4497–4505.

[48] E.K. Lee, W.-K. Jeon, M.Y. Chae, et al., Decreased expression of glutaredoxin 1 is required for transforming growth factor-β1-mediated epithelial–mesenchymal transition of EpRas mammary epithelial cells, Biochem. Biophys. Res. Commun. 391 (1) (2010) 1021–1027.

[49] M. Nousiainen, H.H. Silljé, G. Sauer, et al., Phosphoproteome analysis of the human mitotic spindle, Proc. Natl. Acad. Sci. USA 103 (14) (2006) 5391–5396.

[50] P. Zhang, K. Bill, J. Liu, et al., MiR-155 is a liposarcoma oncogene that targets casein kinase-1α and enhances β-catenin SignalingmiRNA deregulation in human liposarcoma, Cancer Res. 72 (7) (2012) 1751–1762.

[51] Q. Yan, J. Chen, W. Li, et al., Targeting miR-155 to treat experimental scleroderma, Sci. Rep. 6 (1) (2016) 1–11.

[52] X. Li, L. He, Q. Yue, et al., MiR-9-5p promotes MSC migration by activating β-catenin signaling pathway, Am. J. Physiol. Cell Physiol. 313 (1) (2017) C80–C93.

[53] C.-M. Cruciat, C. Dolde, R.E. De Groot, et al., RNA helicase DDX3 is a regulatory subunit of casein kinase 1 in Wnt–β-catenin signaling, Science 339 (6126) (2013) 1436–1441.

[54] V. Anathy, K.G. Lahue, D.G. Chapman, et al., Reducing protein oxidation reverses lung fibrosis, Nat. Med. 24 (8) (2018) 1128–1135.

[55] L. Wang, Y.J. Ahn, R. Asmis, Sexual dimorphism in glutathione metabolism and glutathione-dependent responses, Redox Biol. 31 (2020), 101410.

[56] Y.J. Ahn, L. Wang, S. Tavakoli, et al., Glutaredoxin 1 controls monocyte reprogramming during nutrient stress and protects mice against obesity and atherosclerosis in a sex-specific manner, Nat. Commun. 13 (1) (2022) 790.

[57] N. Congdon, H. Fan, K. Choi, et al., Impact of posterior subcapsular opacification on vision and visual function among subjects undergoing cataract surgery in rural China: study of Cataract Outcomes and Up-Take of Services (SCOUTS) in the Caring is Hip Project, report 5, Br. J. Ophthalmol. 92 (5) (2008) 598–603.

[58] C.S.-U. Fong, P. Mitchell, E. Rochtchina, et al., Three-year incidence and factors associated with posterior capsule opacification after cataract surgery: the Australian Prospective Cataract Surgery and Age-related Macular Degeneration Study, Am. J. Ophthalmol. 157 (1) (2014) 171–179, e171.

[59] J.-S. Lee, C.-C. Chung, K.-K. Lin, et al., Time trends in cataract surgery and after-cataract laser capsulotomy in Taiwan: a population-based retrospective cohort study, Int. J. Surg. 36 (2016) 265–273.

[60] H.A. Tokko, F. Hussain, A. Al-Awadi, et al., Factors associated with the development of posterior capsule opacification requiring yttrium aluminum garnet capsulotomy, Optom. Vis. Sci. 96 (7) (2019) 492–499.